THE JOURNAL OF PHYSICAL CHEMISTRY B

Article

pubs.acs.org/JPCB

Novel Spiropyran Amphiphiles and Their Application as Light-Responsive Liquid Crystalline Components

Kristian J. Tangso,[†] Wye-Khay Fong,[†] Tamim Darwish,[‡] Nigel Kirby,[§] Ben J. Boyd,*[,†] and Tracey L. Hanley*[,‡]

[†]Drug Delivery, Disposition and Dynamics, Monash Institute of Pharmaceutical Sciences, Monash University (Parkville Campus), 381 Royal Parade, Parkville, Victoria 3052, Australia

[‡]Australian Nuclear Science and Technology Organization, Locked Bag 2001, Kirrawee DC, NSW 2232, Australia

[§]SAXS/WAXS Beamline, Australian Synchrotron, Clayton, Victoria, Australia

Supporting Information

ABSTRACT: Light-responsive materials formed by liquid crystalline lipids in water have potential application to drug delivery through inclusion of photochromic additives such as spiropyran. A series of novel analogues of spiropyran (SP) have been synthesized with an SP headgroup that possess a C_8 (SP-OC), C_{12} (SP-L), and C_{16} (SP-P) tail to probe the influence of the length of the hydrophobic tail on their physicochemical properties and effect on behavior in liquid crystal matrices with a view to application as stimulus-responsive elements on ultraviolet irradiation. In addition, compounds possessing an oleyl (SP-OL) and phytanyl (SP-PHYT) tail, to mimic those of the "parent" reverse bicontinuous cubic (V_2) phase forming lipids, glyceryl monooleate (GMO) and phytantriol, were also prepared. The photochromic compounds were characterized by their melting points and photophysical behavior in solution using techniques including hot stage microscopy (HSM), differential scanning calorimetry (DSC), and UV–visible spectroscopy. Their effect on the equilibrium nanostructure of bulk V_2 phases and phase-switching kinetics after exposure to UV light was assessed using small-angle X-ray scattering (SAXS). The melting point of the SP derivatives decreased linearly with increasing chain length, which suggests that interactions between the head groups governed their melting point, rather than the van der Waals interactions between the tails. Changing the R group did not influence the equilibrium rate constants for the isomerization of SP. Phase transition temperatures of liquid crystalline (LC) matrices were influenced significantly by incorporation of the SP derivatives and were greatest when the photochromic compound possessed an intermediate tail length substituent compared to the short alkyl or bulkier moieties. The level of disruption of lipid packing, and hence phase structure, were dependent on the duration of UV exposure.

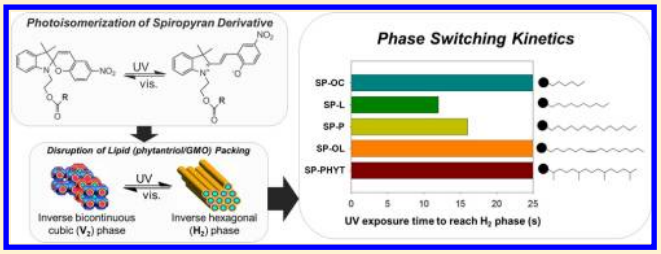

INTRODUCTION

Lipid-based liquid crystalline systems are attracting increasing interest as a means of controlled release drug delivery. When amphiphilic lipids are present in excess water, they can self-assemble into thermodynamically stable liquid crystalline phases (often termed "mesophases" or just "phases").[1−6] The nonlamellar mesophases of most current interest in drug delivery systems are the reversed bicontinuous cubic (V_2) phase and the reversed hexagonal (H_2) phase. Their ability to solubilize hydrophilic, hydrophobic, and amphiphilic drugs make them excellent candidates for use as drug delivery matrices (Figure 1). The most commonly studied lipids for forming V_2 phases in excess water are glyceryl monooleate (GMO) a dietary lipid, and phytantriol, an ingredient commonly used in the cosmetic industry; the chemical structures are illustrated in Figure 1.

Lipid packing within the mesophase structure is a key determinant of the overall nanostructure formed in water and can be influenced by lipid concentration, temperature, pressure, additives, and solvent composition.[7−14] The nanostructure, in turn, is what dictates the rate at which drug is released,[13,15,16] and transitions between phases are of interest for triggering release of incorporated active ingredients.

There are several variables that may be used for triggering phase transitions in situ after administration, including temperature,[13] salt, dilution, and pH.[17,18] Fong et al.[13] demonstrated that temperature-stimulated systems can provide drug release on demand. However, in practice there is potential for accidental activation of drug release in cases where direct application of temperature is used to stimulate the phase change, presenting a major limitation. A possible alternative could be to utilize additives that can induce a phase change in response to a more selective external stimulus such as light.[19−21]

Received: April 18, 2013
Revised: June 7, 2013
Published: August 3, 2013

   dx.doi.org/10.1021/jp403840m | J. Phys. Chem. B 2013, 117, 10203−10210

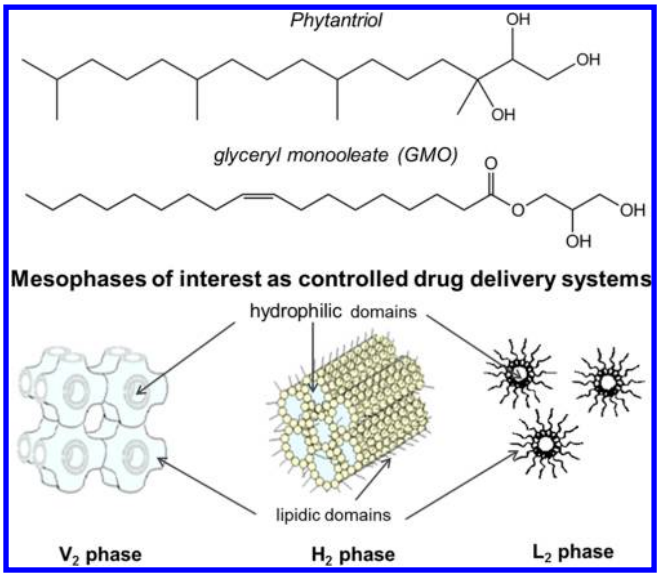

Figure 1. (Top) Chemical structures for phytantriol and glyceryl monooleate (GMO). (Bottom) Structure of the reversed bicontinuous cubic phase (left), the reversed hexagonal phase (center), and inverse micelles (right), indicating compartments within the nanostructure which can encapsulate hydrophilic and hydrophobic drugs.

Rendering liquid crystals light responsive by incorporating photochromic compounds that alter lipid packing upon irradiation may yield novel light-activated "on demand" drug delivery systems with potential to provide a selective and noninvasive approach to delivery in tissues that are not amenable to direct heat activation, such as the posterior section of the eye. Materials such as azobenzenes, spirooxazines, and spiropyrans are families of organic photochromic compounds that undergo reversible isomerization in response to UV irradiation and can be employed to disrupt lipid packing within the LC structure.[22] Although azobenzenes have shown great potential as versatile and tunable components for nanodevices,[23−25] their toxicity remains under question. In contrast, the cytotoxicity of spiropyrans has been tested, and they were found to be safe for application in bionanosensing.[26] Consequently, spiropyrans have recently been of interest for the development of light responsive liquid crystalline nanomaterials.[27]

Spiropyrans reversibly switch between the colorless, nonpolar, closed "spiro" form (SP) and the colored, zwitterionic, open "merocyanine" form (MC) when illuminated with white and UV light, respectively[28−32] (Figure 2). Drummond et al. have synthesized a series of spirobenzopyran derivatives where this equilibrium photochemical and physicochemical behavior was established in solution.[22,31,32] This structural change can be utilized to alter lipid packing, and studies have shown that spiropyran is able to induce phase changes in LC matrices.[1] Fong et al.[1] hypothesized that attachment of an alkyl group to the spiropyran moiety "anchors" the dye into the bilayer structure, thereby improving its ability to disrupt the nanostructure of the mesophase. Incorporation of a laurate derivative of SP (SP-L) into the V_2 phase formed by phytantriol in excess water induced a reversible change between the V_2 and H_2 phases on UV irradiation, whereas underivatized SP had no effect.

It is not known whether the laurate tail is the optimal hydrophobic group to enable anchoring in the mesophase bilayer and disruption of structure on irradiation. To this end, the influence of the hydrophobic group on the physicochemical properties and behavior of spiropyran derivatives in LC matrices was investigated. Novel photochromic amphiphiles possessing C_8 (SP-OC) and C_{16} (SP-P) tails were prepared to complement the previous studies using C_{12} (SP-L), which was resynthesized for the current studies. Amphiphiles possessing oleyl (SP-OL) and phytanyl (SP-PHYT) tails were also synthesized to mimic those of the "parent" V_2 phase forming lipids, glyceryl monooleate (GMO) and phytantriol. The analogues of spiropyran, illustrated in Figure 2, were all assessed for their ability to influence the equilibrium nanostructure of the LC matrices and their efficiency for disruption of lipid packing and subsequent induction of phase switching upon UV irradiation.

MATERIALS AND METHODS

Synthesis. 1-(2-Hydroxyethyl)-3,3-dimethylindolino-6′-nitrobenzopyrylospiran (spiropyran alcohol, SP-OH) was purchased from Tokyo Chemical Industry Co., Ltd. (Tokyo, Japan). Lauric and palmitic acid (98% deuterated) were generously provided by the National Deuteration Facility (Lucas Heights, NSW, Australia). 4-(Dimethylamino)pyridine (DMAP), *N*,*N*′-dicyclohexylcarbodiimide (DCC), and hydrogenated lauric, palmitic, octanoic, and oleic acids were obtained from Sigma-Aldrich (St. Louis, MO). Phytanic acid was a generous gift from CSIRO (Melbourne, Australia). These ingredients were used without further purification. Thin layer chromatography (TLC) was performed on Fluka analytical silica gel aluminum sheets (25 F254) and Davisil silica gel LC60 Å (40−63 μm) was used for flash column chromatography (FCC). Both materials were purchased from Sigma-

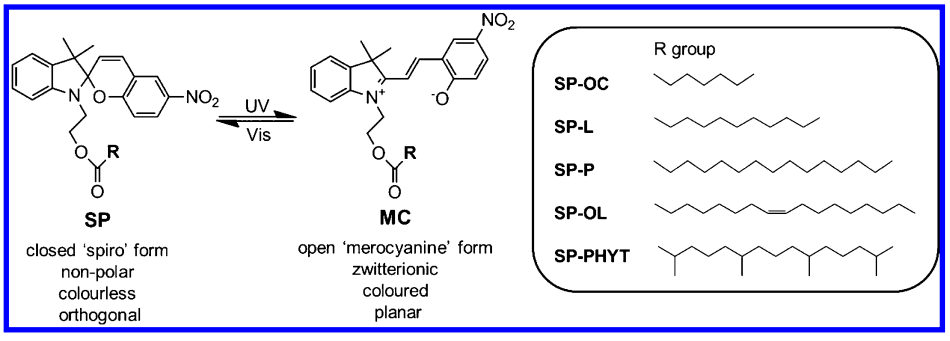

Figure 2. Equilibrium reaction that exists between the stable spiro isomer (SP) and the merocyanine form (MC) in solution. The structures of the R group for each SP derivative are indicated in the legend.

dx.doi.org/10.1021/jp403840m | J. Phys. Chem. B 2013, 117, 10203−10210

Aldrich (St. Louis, MO). Details of the experimental procedure for the synthesis of SP derivatives, which employed standard DCC/DMAP coupling of the acid to the free alcohol on SP-OH, are described in the Supporting Information.

Nuclear Magnetic Resonance (NMR) Spectroscopy. ^{1}H NMR (400 MHz), ^{13}C NMR (100.6 MHz), and ^{2}H NMR (102.6 MHz) spectra were recorded on a Bruker 400 MHz instrument at ca. 25 °C. In ^{1}H NMR spectra, chemical shifts (ppm) were referenced to residual solvent protons (7.26 ppm in $CDCl_3$). In ^{13}C NMR spectra, chemical shifts (ppm) were referenced to the carbon signal of the deuterated solvent (77.0 ppm in $CDCl_3$). NMR spectra of the SP derivatives are shown in the Supporting Information.

Hot Stage Microscopy (HSM). As a preliminary technique, hot stage microscopy (HSM) was used to determine the melting point of the SP derivatives. A small sample of each compound was heated at a rate of 5 °C/min using a Mettler Toledo FP82HT hot stage fitted with a Mettler Toledo FP90 central processor temperature controller. The melting point range was observed under a Zeiss Axiolab E microscope.

Differential Scanning Calorimetry (DSC). To confirm the hot stage microscopic observations, the melting points were also studied using DSC. A Perkin-Elmer DSC 7 fitted with a Thermal Analysis Controller 7/DX was used to measure the transfer of heat energy (enthalpy, ΔH) to or from the sample (2−6 mg) as the temperature was raised from 25 to 120 °C at a rate of 10 °C/min.

UV−Visible Spectroscopy. UV−visible absorption spectra were measured on a Varian Cary-50 Bio spectrophotometer (Melbourne, Australia) fitted with a Peltier temperature control cell from 200 to 800 nm at a scan rate of 600 nm s^{-1} and kinetic measurements at 540 nm. Solutions for UV−visible measurements were prepared to concentrations of 2.0×10^{-4} M in methanol. White light and UV illuminations were conducted using a white light torch and a 12 LED ultraviolet 380 nm torch, respectively.

Lipids. Myverol 18-99K from Kerry Ingredients (Almere, The Netherlands) was used as a substitute for GMO for its relatively low cost and similar phase behavior to pure GMO.[33] The composition of Myverol 18-99K has been described in detail previously.[34] Phytantriol was a gift from DSM Nutritional Products Ltd., Germany, with a minimum purity of 95%. Milli-Q grade water purified through a Milli-pore system was used throughout this study.

Preparation of Bulk Liquid Crystalline Samples ("Bulk Phases"). Various concentrations (mol % relative to lipid) of each SP derivative were dissolved in lipid. The aqueous phase, either Milli-Q water or phosphate buffer solution (PBS) controlled at pH 7.4, and lipid component (2:1, v:v) were thoroughly mixed by heating transiently to approximately 60 °C and vortex mixing to homogeneity for at least three cycles. Bulk phases were then left to equilibrate on a tube roller at 25 °C for at least 48 h prior to analysis.

Structural Characterization of Bulk Phases Using Small-Angle X-ray Scattering (SAXS). *Equilibrium Phase Diagrams.* For comparison of phase transition temperatures and the generation of phase diagrams, two different SAXS setups were utilized for phytantriol (Figure 6) and GMO (Figure 7) systems, respectively.

Phytantriol-based bulk phase samples were loaded into a flat stainless steel metal plate (96 sample positions with a thickness of 0.5 mm) sealed on both sides with Kapton tape, which was attached to a thermostated heating block and mounted on the SAXS/WAXS beamline at the Australian Synchrotron (AS). The holder was allowed to equilibrate at 28 °C for at least 30 min before acquiring the first scattering pattern, with 10 min equilibration at each 2.5 ± 0.1 °C temperature increment from 28 to 75 °C. Radiation with wavelength (λ) of 1.0322 Å (12 keV) was selected and an acquisition time of 0.5 s was used. The 2D scattering patterns were collected on a 1 M Pilatus detector, which covered the q range of interest from 0.0021 to 0.0986 Å where $q = 4\pi \sin(\theta/\lambda)$ and θ is the scattering angle.

GMO-based bulk phase samples were packed into quartz glass capillaries (Capillary Tube Supplies Ltd., Germany) with a path length of 2.0 mm, sealed with wax, and then inserted into a thermostated metal heating block controlled by a Peltier system accurate to ± 0.1 °C. The samples were introduced to the beam of a Bruker Nanostar SAXS camera, with pinhole collimation for point focus geometry. The instrument source was a copper rotating anode (0.3 m filament) operating at 45 keV and 110 mA, fitted with Montel mirrors, resulting in Cu Kα radiation wavelength 1.54 Å. The SAXS camera was fitted with a Vantec 2000 2D detector (effective pixel size 550 μm) which was located 700 mm from the sample to provide a q-range of 0.008−0.35 Å^{-1}. Samples were equilibrated for 15 min (previously determined as an appropriate equilibration period these sample in this apparatus with incremental temperature changes), and scattering patterns were collected over 15 min under vacuum to minimize air scattering. Samples were heated stepwise from 20 to 65 °C at 3 °C increments.

Dynamic Irradiation Experiments. Time-resolved irradiation experiments using synchrotron SAXS were conducted to assess the efficiency and reversibility of phase transitions induced by these SP derivatives.[35]

Bulk sample matrices prepared in PBS (pH ∼7.4) containing varying concentrations (0.5, 1.0, or 1.5 mol %) of photochromic additive were loaded into 1 mm quartz capillaries and irradiated with UV light (60 mW, 375 nm) at different exposure times: 15, 30, or 60 s. The UV light was delivered to the samples using an EXFO Acticure 4000 UV lamp and fiber optic cable, with the end of the fiber optic cable positioned approximately 5 cm from the sample at a slight tangent to the X-ray beam. The irradiation studies were conducted at hutch temperature (∼30 °C) at the SAXS/WAXS beamline at the Australian Synchrotron. The 2D scattering patterns were acquired every 2 s for the first 2 min, then every minute until the system reverted back to the "starting phase", using a 1 M Pilatus detector (active area 169 × 179 mm^2 with a pixel size of 172 μm) which was located 956 mm from the sample position.

The computer software ScatterBrain Analysis was used to reduce 2D scattering patterns to the one-dimensional scattering function $I(q)$. The d-spacing of the liquid crystalline lattice is derived from Bragg's law ($2d \sin\theta = n\lambda$), where n is an integer, λ is the wavelength, and θ is the scattering angle). Since the scattering profiles of the V_2, H_2, and L_2 phases have been well characterized using SAXS, observing the difference in relative positions of the Bragg peaks, correlated by the Miller indices of known phases, we can confirm the phase identity of the system being analyzed. The V_{2D} phase has the Bragg reflections $\sqrt{2}:\sqrt{3}:\sqrt{4}:\sqrt{6}:\sqrt{8}:\sqrt{9}$, etc., while the H_2 phase can be identified by the Bragg reflections $1:\sqrt{3}:\sqrt{4}$, etc. The L_2 is identified by a singular characteristic broad peak. The absolute location of the peaks allows for the calculation of mean lattice parameter, a, of the matrices, from the corresponding interplanar distance, d ($d = 2\pi/q$), using the appropriate scattering law for the phase structure. For cubic phases, a =

$d(h^2 + k^2 + l^2)^{1/2}$, while for the H_2 phase, $a = 4d/3(h^2 + k^2)^{1/2}$, where h, k, and l are the Miller indices for the particular structure present. Since the L_2 phase shows only one broad peak, d is termed the characteristic distance.[36]

RESULTS AND DISCUSSION

Synthesis of the SP Derivatives. Five SP derivatives were successfully synthesized and are detailed in Figure 2. Full synthesis details are contained in the Supporting Information. ^{1}H and ^{13}C NMR spectroscopy was used to characterize the synthesized derivatives. As no uncharacteristic peaks were observed in the ^{1}H and ^{13}C NMR spectra for the hydrogenated SP derivatives and the ^{2}H NMR spectra for the deuterated form of selected SP moieties, the estimated purity of the synthesized spiropyrans is >98% (see Darwish et al., Supporting Information, Table SI1, for comparison, where chemical shifts for *n*-propanol spiropyran are listed).[28]

Melting Points of the SP Derivatives. DSC thermograms of the SP derivatives are illustrated in the Supporting Information. The melting points of the SP derivatives decreased approximately linearly with increasing chain length (Figure 3).

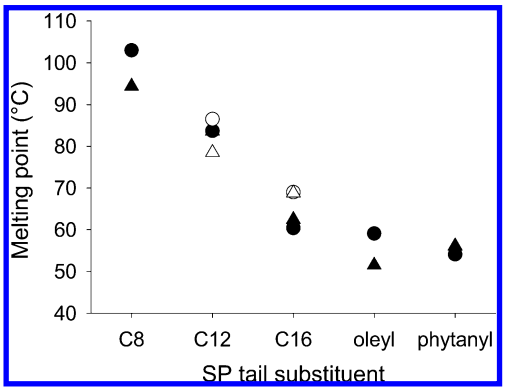

Figure 3. Influence of chain length/size on the melting point of SP-OC, SP-L, SP-P, SP-OL, and SP-PHYT determined by hot stage microscopy (circles) and differential scanning calorimetry (triangles). The melting points of the deuterated compounds are denoted by unfilled symbols. Plotted values represent the "onset" melting temperature.

This rather counterintuitive finding was in agreement for both independent methods (HSM and DSC). Usually increasing the chain length in a homologous series leads to an increase in melting point due to increased intermolecular van der Waals forces between the molecules. The interesting trend shown in Figure 3 therefore suggests that interactions between the head groups rather than the hydrophobic tails might be governing the melting point. Space-filling models for the derivatives are illustrated in Figure 4. It is not immediately apparent why the longer chain alkyl derivatives necessarily might pack less strongly than the short octanoate derivative, because the chain is quite separate from the head structure in this representation and neighboring chains might be expected to interact more extensively than the C_8 derivative. It is therefore likely that the chain adopts a bulky conformation and disrupts the hydrogen bonding between adjacent headgroups. In the case of similar amphiphiles with sugar head groups, regioisomers and chirality has also been shown to provide seemingly anomalous melting behavior, but in those compounds it is clear that they form lamellar structures in the solid state.[37] The neat SP derivatives were not birefringent when observed under crossed polarized microscope, precluding the likelihood of lamellar structure.

On the other hand, the oleyl and phytanyl derivatives do appear to present a bulky, convoluted structure and compromised packing might reasonably be expected with consequent lower melting points. A number of deuterated versions of the SP derivatives were prepared with a view to their use in future small-angle neutron scattering studies. To provide a more complete data set, their behavior has been pooled and described with that of the hydrogenated derivatives. The deuterated compounds demonstrated similar behavior in their melting point to their hydrogenated equivalents, with a slightly higher onset melting temperature.

Photophysical Behavior of SP Derivatives. The rate at which the SP headgroup switches between the closed and open form in response to UV and visible irradiation is indicative of their photochromic behavior in solution. In the absence of UV irradiation, a chemical equilibrium exists between the open merocyanine form (MC) of spiropyran and the closed spiro form (SP), as depicted in Figure 2, with the latter isomer being more abundant. When a solution of spiropyran is excited with UV light, the equilibrium between the two isomers is shifted to favor MC, which is made evident when the solution strengthens in color as the concentration of MC increases. After irradiation, MC switches back to SP. This process can easily be followed by the visible absorption of MC as a function of time.

The observed equilibrium rate constants for the isomerization of photochromic compounds in methanol were found to be comparable (Table 1, Figure 5). This implies that the R group on the structure of the SP derivative does not significantly influence the isomerization rate, and thus it can be deduced that changes in bulk phase structure during irradiation would not be due to differences in the photophysical properties of the SP derivative, but is directly indicative of disruption of structure caused by geometric changes in the structure of the additive. An example of the spectral changes of SP-P in methanol at 25 °C immediately after UV irradiation and white light illumination and a description of how the isomerization rates were calculated can be found in the Supporting Information. For SP-L the rate of isomerization in the V_2 liquid crystalline matrices has been previously shown to be the same as in methanol.[1]

Effect of SP Derivatives on the Equilibrium Nanostructure of Bulk Phytantriol and GMO Reverse Bicontinuous Cubic Phases. In agreement with previous studies on SP-L,[1] incorporation of SP compounds into bulk V_2 phases prepared using phytantriol (Figure 6) and GMO (Figure 7) lowered the transition temperature to the H_2 phase to varying degrees in the absence of UV irradiation. Determination of the phase transition temperature is an important consideration in designing the optimal formulation that requires a minimal concentration of photochromic compound, possesses a phase transition temperature close to physiological temperature, and requires minimal UV exposure.

The bulk phytantriol-based cubic phase containing SP-OC (Figure 6A) existed as V_2 phase up to 5 mol % of the additive and there was no significant change in the phase transition temperatures with increasing concentration of photochromic. This suggests that the C_8 tail has insignificant impact on the lipid packing within the LC and a large amount of the additive might be necessary to disrupt the liquid crystalline structure on irradiation.

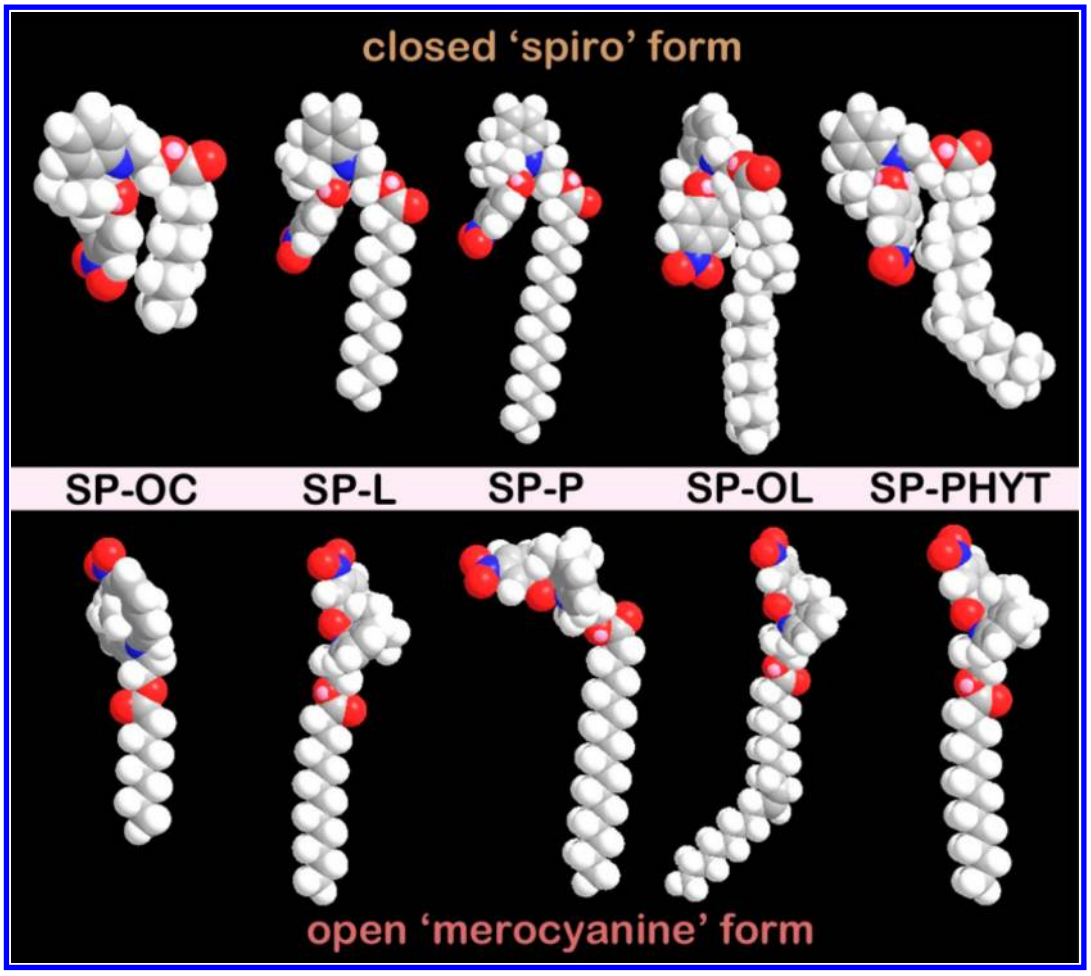

Figure 4. Space-filling models of the spiropyran derivatives in the closed form prior to UV irradiation (top panel) and the open form after exposure to UV light (bottom panel) arranged in their lowest energy state, as predicted in Chem3D Pro 12.0.

Table 1. Observed Equilibrium Rate Constants for Isomerization of SP Derivatives in Methanol at 2.0 × 10^{-4} M (mean ± s.d., n = 1−3)[a]

photochromic	k_1 (after white light) ×10^{-4} s^{-1}		k_2 (after UV light) ×10^{-4} s^{-1}	
SP-OC (h)	○	8.2	●	7.3
SP-L (h)		6.1 ± 0.5		5.1 ± 0.1
SP-L (d)	△	7.0	▲	4.2
SP-P (h)		7.1 ± 1.4		5.0 ± 0.05
SP-P (d)	□	11.7	■	7.7
SP-OL (h)	+	17.7	+	8.3
SP-PHYT (h)	×	12.8	×	9.1

[a]Symbol key included in support of Figure 6.

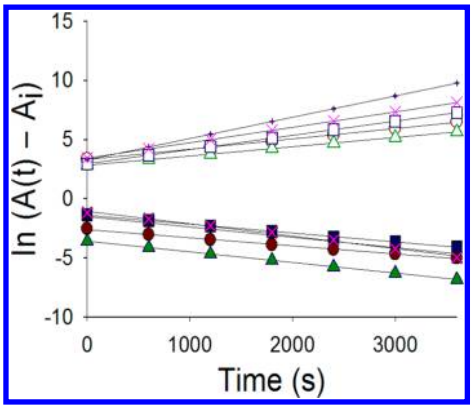

Figure 5. First-order growth and decay of MC form after exposure to 5 min white and UV light, respectively; absorbances measured at 540 nm. Refer to Table 1 for what symbols correspond to.

In comparison, SP-L, which possessed an intermediate length C_{12} tail, caused a slight lowering of the phase transition temperature when incorporated into the phytantriol LC matrix (Figure 6B). This was apparent at >1 mol % of SP-L, where the V_2 structure coexisted with the H_2 phase near physiological temperature. It can be inferred that when incorporated at these concentrations SP-L would provide sufficient lipid packing disruption to induce $V_2 \rightarrow H_2$ phase transition at close to ∼37 °C on application of UV irradiation. This is consistent with the behavior observed in the study reported by Fong et al.[1] At >1.5 mol % the V_2 phase did not exist without the coexisting H_2 phase, and hence there is an upper limit for the amount that could be added without compromising the structure of the "initial phase".

SP-P has a slightly longer tail (C_{16}) than SP-L, but displayed similar phase behavior (Figure 6C) with the phase transition temperatures being suppressed to close to physiological temperature in the presence of 1.5 mol % of the palmitate derivative.

Incorporation of SP analogues with an unsaturated (oleyl) and highly branched (phytantriol) tail into the phytantriol-

dx.doi.org/10.1021/jp403840m | J. Phys. Chem. B 2013, 117, 10203−10210

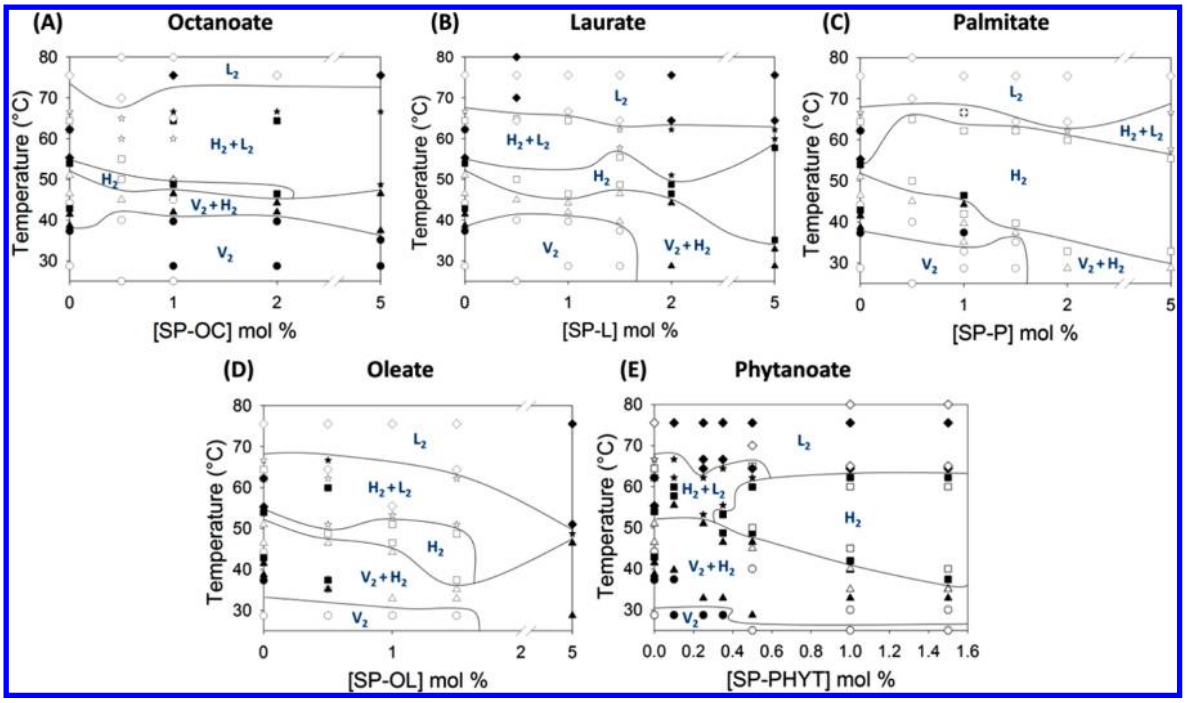

Figure 6. Effect of the spiropyran derivatives on the equilibrium nanostructure of bulk phytantriol-based V_2 phases upon heating in the absence of UV irradiation. Bulk phases were heated stepwise from 20 to 65 °C at 3 °C increments and LC structures characterized by SAXS. Panels A–E are temperature vs concentration phase diagrams of bulk phytantriol LC containing different amounts of photochromic additive, SP-OC, SP-L, SP-P, SP-OL, and SP-PHYT, respectively. Estimated phase boundary lines are drawn to outline regions where samples exists as V_2 phase (●), coexisting V_2 and H_2 phases (▲), H_2 phase (■), and coexisting H_2 and L_2 phases (★) and L_2 phase (♦). Samples were prepared either in Milli-Q water (filled shapes) or in PBS at pH 7.4 (unfilled shapes).

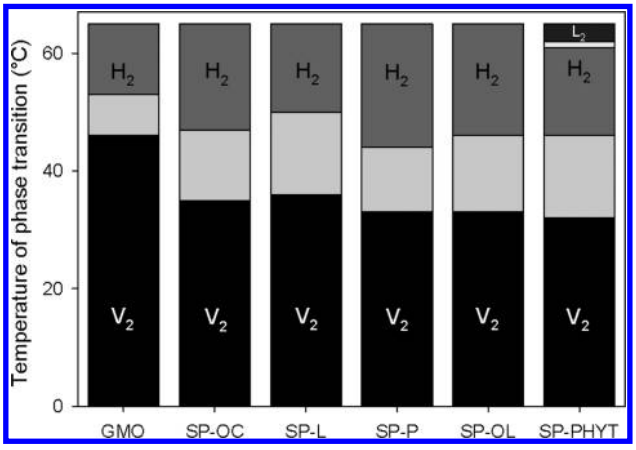

Figure 7. Influence of photochromic additive on the phase behavior of GMO-based bulk cubic phase upon heating in the absence of UV irradiation. Bulk phases were heated stepwise from 20 to 65 °C at 3 °C increments and LC structures characterized by SAXS.

based LC resulted in a dramatic lowering of the phase transition temperatures. In both cases, a very small fraction of additive (<0.5 mol %) suppressed the phase transition temperatures to well below physiological temperature (Figure 6D,E). At >0.5 mol % SP-PHYT the cubic phase did not exist at the lowest temperature studied. This supports the hypothesis that a tail with a similar structure to the parent lipid, phytantriol, would enhance the miscibility between the two components and, consequently, SP-PHYT provided the most disruption to the lipid packing in the LC matrix.

In the case of GMO, the effect of the different SP derivative was only studied at a single concentration (1 mol %). Although the phase transition temperatures in the presence of the SP derivatives were suppressed by approximately 5 °C compared to GMO alone, no significant differences between the transition temperatures were observed on addition of the five SP derivatives (Figure 7). It should be noted that the transition temperatures for GMO alone are ∼10 °C higher than for phytantriol, and hence the sensitivity to small amounts of the additives may be reduced.

These experiments indicate that most of the systems introduced here have the potential to undergo a phase transition on irradiation of the photochromic additive with UV light when incorporated at an appropriate concentration.

Phase-Switching Kinetics of Phytantriol and GMO Cubic Phases Using with Photochromic Compounds after Exposure to UV Light. As recently reported,[1] SP-L was able to induce reversible isothermal phase switching of cubic phase to the H_2 phase in response to UV irradiation.

As mentioned earlier, in addition to identification of the phase present in a given sample, information related to its lattice parameter (LP) can also be deduced from SAXS scattering profiles.[36] In the case where heat is generated on irradiation, such as NIR irradiation in the presence of gold nanorods, the equilibrium LP versus temperature plots can be used as a calibration plot to derive the "apparent temperature" felt by the matrix which is a consequence of the disruption of lipid packing due to temperature in the dynamic experiments.[38,39]

In the case of photochromic compounds and the effect of UV irradiation on their ability to disrupt lipid packing, the degree of disruption can by analogy be considered as an "equivalent temperature" T_{equiv}. Consequently, from the temperature scans conducted to produce the phase behavior diagrams of the LC

systems loaded with the photochromic compounds, LP versus temperature calibration plots were also generated; an example for SP-OC is shown in the Supporting Information. Using these calibration curves, the equivalent temperature was extrapolated for each scattering profile obtained at every time point throughout the dynamic irradiation experiments. Therefore, the phase-switching kinetics across changes in experimental variables can be compared using T_{equiv} versus time profiles, as illustrated in Figure 8. It must be noted again that it is not the

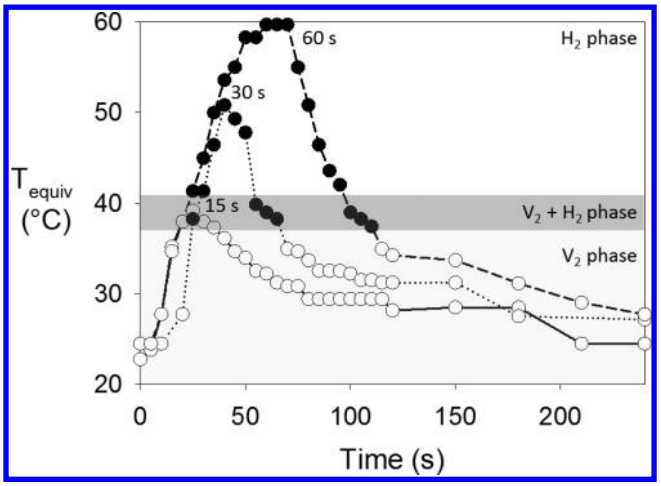

Figure 8. Effect of different UV exposure times on the phase-switching kinetics of phytantriol-based LC matrices containing 1 mol % SP-OC as representative of profiles providing the data in Table 2 for the other derivatives.

thermal motion that is inducing a change in nanostructure, but rather the disruption to the matrix caused by photoisomerization of the spiropyran moieties in response to UV irradiation.

The duration of UV exposure has been shown to influence the extent to which phase the LC matrix transitions to, as well as its phase-switching kinetics (Figure 8). The 1 mol % SP-OC phytantriol-based LC system, in this example, gave rise to a mixed $V_2 + H_2$ after only 15 s of UV "on", and after 30 s of UV exposure the LC transitioned completely to the H_2 phase, and relaxed back to the initial phase on removal of UV light. As depicted in Table 2, prolonged UV exposure can lead to phase transitions from V_2 to H_2 and even up to the L_2 phase, indicating significant capacity in the isomerization of the SP derivatives to provide a range of disruption ability depending on the degree of isomerization.

The selection of the optimal light-responsive system was based on rapid switching to the H_2 phase, and possessing maximum T_{equiv} above and closest to physiological temperature (~37 °C). The sample containing 1 mol % SP-L therefore met the desired properties of the optimal light-activated LC system. The phytantriol structure possesses a C_{13} side chain with a kink. The similarity in hydrophobic length between phytantriol and the C_{12} alkyl tail rationalizes the proposal that SP-L is best matched structurally to occupy space within the phytantriol bilayer structure and provide the greatest disorder to the lipid packing upon UV irradiation. Further modeling of this mechanism is essential to gain a better understanding as to why the various spiropyran derivatives display different lipid phase-switching kinetics.

The photoresponsive LC systems introduced here have shown to be promising candidates for light-activated drug

Table 2. Efficiency of SP Derivatives To Induce Phase Switching in Bulk Phytantriol-Based LC upon UV Irradiation, and Comparison of Time (s) To Reach Maximum Equivalent Temperature (T_{equiv}) and Respective Mesophase(s) Reached for Samples Loaded with Varying Concentration of Photochromic Additive at pH ~7.4 and Different UV Exposure Times

photochromic	concn (mol %)	UV exposure time (s)	max T_{equiv} (°C)	time to max T_{equiv} (s)	final mesophase
SP-OC	0.5	15	43.0	15	$V_2 + H_2$
		30	59.5	26	H_2
		60	64.5	47	L_2
	1.0	15	39.2	25	V_2
		30	50.8	40	H_2
		60	59.7	60	H_2
SP-L	0.5	15	35.3	9	$V_2 + H_2$
		30	55.3	19	H_2
		60	68.8	45	$H_2 + L_2$
	1.0	15	47.3	12	H_2
		30	55.3	27	H_2
		60	58.8	50	L_2
	1.5	15	34.1	19	$V_2 + H_2$
		30	55.2	25	$H_2 + L_2$
		60	56.7	56	L_2
SP-P	0.5	15	41.8	23	$V_2 + H_2$
		30	61.1	27	H_2
		60	68.5	57	$H_2 + L_2$
	1.0	15	36.3	16	H_2
		30	51.9	27	H_2
		60	–	–	L_2
	1.5	15	58.8	18	H_2
		30	–	–	–
		60	–	–	–
SP-OL	1.0	15	29.3	25	H_2
		30	40.1	35	H_2
		60	50.7	60	L_2
	1.5	15	44.0	13	H_2
		30	56.9	23	H_2
		60	60.2	54	L_2
SP-PHYT	0.5	15	44.7	20	H_2
		30	62.0	25	H_2
		60	68.9	56	L_2
	1.0	15	38.8	25	H_2
		30	54.1	30	H_2
		60	–	–	–
	1.5	15	52.5	13	H_2
		30	–	–	–
		60	–	–	–

delivery, and similar experiments are underway to explore spiropyran–LC systems that reversibly switch from a slow releasing matrix to fast releasing matrix upon UV irradiation (e.g., H_2 or L_2 to V_2).[16] As UV penetration through biological material is generally limited, preliminary studies are also in progress that utilize NIR light as an alternate light source for its greater penetration depth (up to ~50 mm).[40] Upconverting nanoparticles (UCNPs) emit UV light in response to NIR light exposure. These particles can be incorporated into the optimal spiropyran-containing LC matrices to selectively induce phase transitions.

dx.doi.org/10.1021/jp403840m | J. Phys. Chem. B 2013, 117, 10203–10210

CONCLUSION

Novel amphiphilic spiropyran derivatives with different hydrophobic tail structures were synthesized. For the alkylated derivatives, their melting points showed an inverse dependence with tail length, indicating that the headgroup interactions dominate the solid-state behavior. The photophysical behavior in methanol was invariant with hydrophobe structure. Inclusion of the photochromic additives into both phytantriol- and GMO-based bulk V_2 phases lowered the phase transition temperature to the H_2 phase. The prolonged irradiation of these systems with UV-light-induced phase switching from the $V_2 \rightarrow H_2 \rightarrow L_2$ phases. Spiropyran laurate (SP-L) represents a novel effective photochromic additive for imparting light responsiveness to lipid-based liquid crystalline drug delivery systems.

ASSOCIATED CONTENT

Supporting Information

Details on the synthesis of the spiropyran derivatives, ^{1}H, ^{2}H, and ^{13}C NMR spectroscopy characterizations (including spectra) of the different species, DSC thermograms, UV−vis spectroscopy, and SAXS studies. This material is available free of charge via the Internet at http://pubs.acs.org.

AUTHOR INFORMATION

Corresponding Author

*E-mail: ben.boyd@monash.edu (B.J.B.); tracey.hanley@ansto.gov.au (T.L.H.).

Notes

The authors declare no competing financial interest.

ACKNOWLEDGMENTS

The authors acknowledge the Australian Institute of Nuclear Science and Engineering for funding this project (ALNGRA11161). K.J.T. also thanks AINSE for support in the form of an Honours stipend and W.-K.F. thanks AINSE for a PGRA scholarship. B.J.B. acknowledges the Australian Research Council for a Future Fellowship. Part of this work was conducted at the SAXS/WAXS beamline at the Australian Synchrotron, Victoria, Australia.

REFERENCES

(1) Fong, W.-K.; Malic, N.; Evans, R.; Hawley, A.; Boyd, B.; Hanley, T. *Biointerphases* **2012**, *7*, 1−5.
(2) Boyd, B.; Dong, Y.; Rades, T. *J. Liposome Res.* **2009**, *19*, 12−28.
(3) Larsson, K. *J. Phys. Chem.* **1989**, *93*, 7304−7314.
(4) Kaasgaard, T.; Drummond, C. J. *Phys. Chem. Chem. Phys.* **2006**, *8*, 4957−4975.
(5) Larsson, K. *J. Dispersion Sci. Technol.* **1999**, *20*, 27−34.
(6) Larsson, K.; Fontell, K.; Krog, N. *Chem Phys Lipids* **1980**, *27*, 321−328.
(7) Boyd, B.; Whittaker, D.; Khoo, S.; Davey, G. *Int. J. Pharm.* **2006**, *309*, 218−226.
(8) Fontell, K. *Colloid Polym. Sci.* **1990**, *268*, 264−285.
(9) Clogston, J.; Caffrey, M. *J. Controlled Release* **2005**, *107*, 99−111.
(10) Shah, J.; Sadhale, Y.; Chilukuri, D. *Adv. Drug Delivery Rev.* **2001**, *47*, 229−50.
(11) Hyde, S. T.; Andersson, S.; Ericsson, B.; Larsson, K. *Z. Kristallogr.* **1984**, *168*, 213−219.
(12) Engström, S.; Engström, L. *Int. J. Pharm.* **1992**, *79*, 113−122.
(13) Fong, W.-K.; Hanley, T.; Boyd, B. J. *J. Controlled Release* **2009**, *135*, 218−226.
(14) Dong, Y.-D.; Larson, I.; Hanley, T.; Boyd, B. J. *Langmuir* **2006**, *22*, 9512−9518.
(15) Lee, K. W. Y.; Nguyen, T.-H.; Hanley, T.; Boyd, B. J. *Int. J. Pharm.* **2009**, *365*, 190−199.
(16) Phan, S.; Fong, W.-K.; Kirby, N.; Hanley, T.; Boyd, B. J. *Int. J. Pharm.* **2011**, *421*, 176−182.
(17) Negrini, R.; Mezzenga, R. *Langmuir* **2011**, *27*, 5296−5303.
(18) Malmsten, M. *J. Dispersion Sci. Technol.* **2007**, *28*, 63−72.
(19) Eastoe, J.; Zou, A.; Espidel, Y.; Glatter, O.; Grillo, I. *Soft Matter* **2008**, *4*, 1215−1218.
(20) Zou, A.; Eastoe, J.; Mutch, K.; Wyatt, P.; Scherf, G.; Glatter, O.; Grillo, I. *J. Colloid Interface Sci.* **2008**, *322*, 611−616.
(21) Bhattacharya, S.; Bajaj, A. *Chem. Commun.* **2009**, *0*, 4632−4656.
(22) Drummond, C. J.; Furlong, D. N.; Georgaklis, G. *J. Chem. Soc., Faraday Trans.* **1990**, *86*, 3913−3918.
(23) Ikeda, T.; Tsutsumi, O. *Science* **1995**, *268*, 1873−1875.
(24) Liu, Z. F.; Hashimoto, K.; Fujishima, A. *Nature* **1990**, *347*, 658−660.
(25) Blanchard, P. M.; Mitchell, G. R. *Appl. Phys. Lett.* **1993**, *63*, 2038.
(26) Movia, D.; Prina-Mello, A.; Volkov, Y.; Giordani, S. *Chem. Res. Toxicol.* **2010**, *23*, 1459−1466.
(27) Tong, R.; Hemmati, H. D.; Langer, R.; Kohane, D. S. *J. Am. Chem. Soc.* **2012**, *134*, 8848−8855.
(28) Darwish, T. A.; Evans, R.; James, M.; Malic, N.; Triani, G.; Hanley, T. L. *J. Am. Chem. Soc.* **2010**, *132*, 10748−55.
(29) Darwish, T. A.; Evans, R. A.; Hanley, T. L. *Dyes Pigments* **2012**, *92*, 817−824.
(30) Eastoe, J.; Vesperinas, A. *Soft Matter* **2005**, *1*, 338−347.
(31) Drummond, C. J.; Albers, S.; Furlong, D. N.; Wells, D. *Langmuir* **1991**, *7*, 2409−2411.
(32) Drummond, C. J.; Furlong, D. N. *J. Chem. Soc., Faraday Trans.* **1990**, *86*, 3613−3621.
(33) Clogston, J.; Rathman, J.; Tomasko, D.; Walker, H.; Caffrey, M. *Chem. Phys. Lipids* **2000**, *107*, 191−220.
(34) Dong, Y.-D.; Dong, A. W.; Larson, I.; Rappolt, M.; Amenitsch, H.; Hanley, T.; Boyd, B. J. *Langmuir* **2008**, *24*, 6998−7003.
(35) Bakeev, K. N.; Shu, Y. M.; Zezin, A. B.; Kabanov, V. A.; Lezov, A. V.; Mel'nikov, A. B.; Kolomiets, I. P.; Rjumtsev, E. I.; MacKnight, W. J. *Macromolecules* **1996**, *29*, 1320−1325.
(36) Hyde, S. T. In *Handbook of Applied Surface and Colloid Chemistry*; Holmberg, K., Ed.; 2001; Chapter 16, pp 299−332.
(37) Boyd, B. J.; Drummond, C. J.; Krodkiewska, I.; Grieser, F. *Langmuir* **2000**, *16*, 7359−7367.
(38) Fong, W.-K.; Hanley, T. L.; Thierry, B.; Kirby, N.; Boyd, B. J. *Langmuir* **2010**, *26*, 6136−6139.
(39) Fong, W.-K.; Hanley, T. L.; Thierry, B.; Kirby, N.; Waddington, L. J.; Boyd, B. J. *Langmuir* **2012**, *28*, 14450−14460.
(40) Zhan, Q.; Qian, J.; Liang, H.; Somesfalean, G.; Wang, D.; He, S.; Zhang, Z.; Andersson-Engels, S. *ACS Nano* **2011**, *5*, 3744−3757.